Effects of Ni substitution on multiferroic properties in $Bi_5FeTi_3O_{15}$ ceramics

Hui Sun(孙慧), Jiaying Niu(钮佳颖), Haiying Cheng(成海英), Yuxi Lu(卢玉溪), Zirou Xu(徐紫柔), Lei Zhang(张磊), and Xiaobing Chen(陈小兵)

Citation: Chin. Phys. B, 2021, 30 (**10**): 107701. DOI: 10.1088/1674-1056/ac1b92
Journal homepage: http://cpb.iphy.ac.cn; http://iopscience.iop.org/cpb

What follows is a list of articles you may be interested in

Irradiation behavior and recovery effect of ferroelectric properties of PZT thin films

Yu Zhao(赵瑜), Wen-Yue Zhao(赵文悦), Dan-Dan Ju(琚丹丹), Yue-Yue Yao(姚月月), Hao Wang(王豪), Cheng-Yue Sun(孙承月), Ya-Zhou Peng(彭亚洲), Yi-Yong Wu(吴宜勇), and Wei-Dong Fei(费维栋)

Chin. Phys. B, 2021, 30 (**10**): 107702. DOI: 10.1088/1674-1056/ac0dad

Sr-doping effects on conductivity, charge transport, and ferroelectricity of $Ba_{0.7}La_{0.3}TiO_3$ epitaxial thin films

Qiang Li(李强), Dao Wang(王岛), Yan Zhang(张岩), Yu-Shan Li(李育珊), Ai-Hua Zhang(张爱华), Rui-Qiang Tao(陶瑞强), Zhen Fan(樊贞), Min Zeng(曾敏), Guo-Fu Zhou(周国富), Xu-Bing Lu(陆旭兵), and Jun-Ming Liu(刘俊明)

Chin. Phys. B, 2021, 30 (**2**): 027701. DOI: 10.1088/1674-1056/abc15a

Structures and local ferroelectric polarization switching properties of orthorhombic $YFeO_3$ thin film prepared by a sol-gel method

Runlan Zhang(张润兰), Shuaishuai Li(李帅帅), Changle Chen(陈长乐), Li-An Han(韩立安), Shanxin Xiong(熊善新)

Chin. Phys. B, 2019, 28 (**3**): 037701. DOI: 10.1088/1674-1056/28/3/037701

Emergent ferroelectricity in disordered tri-color multilayer structure comprised of ferromagnetic manganites

Li-Wei Niu(牛利伟), Chang-Le Chen(陈长乐), Xiang-Lei Dong(董祥雷), Hui Xing(邢辉), Bing-Cheng Luo(罗炳成), Ke-Xin Jin(金克新)

Chin. Phys. B, 2016, 25 (**10**): 107701. DOI: 10.1088/1674-1056/25/10/107701

First-principles study of the relaxor ferroelectricity of $Ba(Zr, Ti)O_3$

Yang Li-Juan, Wu Ling-Zhi, Dong Shuai

Chin. Phys. B, 2015, 24 (**12**): 127702. DOI: 10.1088/1674-1056/24/12/127702

Effects of Ni substitution on multiferroic properties in $Bi_5FeTi_3O_{15}$ ceramics

Hui Sun(孙慧)[1,3,†], Jiaying Niu(钮佳颖)[1], Haiying Cheng(成海英)[2], Yuxi Lu(卢玉溪)[1], Zirou Xu(徐紫柔)[1], Lei Zhang(张磊)[1], and Xiaobing Chen(陈小兵)[1]

[1] *College of Physics Science and Technology, Yangzhou University, Yangzhou* 225002, *China*
[2] *School of Sino-German Engineering, Shanghai Technical Institute of Electronics & Information, Shanghai* 201411, *China*
[3] *National Laboratory of Solid State Microstructures, Nanjing University, Nanjing* 210093, *China*

(Received 2 July 2021; revised manuscript received 31 July 2021; accepted manuscript online 7 August 2021)

The single-phase multiferroic $Bi_5Fe_{1-x}Ni_xTi_3O_{15}$ (BFNT-x, $x = 0$, 0.1, 0.2, 0.3, 0.4, and 0.5) ceramics were synthesized by a sol-gel auto-combustion method, and their microstructures, ferroelectric, magnetic, and dielectric properties were investigated in detail. All samples belong to layer-perovskited Aurivillius phase containing four perovskite units sandwiched between two Bi–O layers. Ni substitution can not only improve ferroelectricity but also enhance the magnetic properties. The BFNT-0.2 sample shows the largest remnant polarization ($2P_r \sim 11.6$ μC/cm^2) and the highest remnant magnetization ($2M_r \sim 0.244$ emu/g). The enhancement of the magnetic properties may mainly originate from the spin canting of Fe/Ni-O octahedra via Dzyaloshinskii–Moriya (DM) interaction. In order to explore the influence of valance state of magnetic ions on the properties, the x-ray photoelectron spectroscopy was carried out. Furthermore, structural, ferroelectric, and magnetic transitions were also investigated.

Keywords: layer-perovskited oxides, ferroelectricity, weak ferromagnetism, phase transition

PACS: 77.80.–e, 77.80.B–, 91.60.Pn, 75.47.Lx **DOI:** 10.1088/1674-1056/ac1b92

1. Introduction

Single-phase multiferroics refer to those oxides simultaneously exhibiting ferroelectric (FE), ferromagnetic (FM), and/or ferroelastic properties, which have been widely investigated owing to their potential application in transducers, digital memories, and data storages.[1–4] Nevertheless, it is still a challenge to pursue room-temperature (RT) multiferroics because there is rare multiferroics in nature due to the exclusion between ferroelectricity and ferromagnetism.[5–7]

By combining magnetic units with ferroelectric matrices at atomic scale, the single-phase multiferroics can be obtained. Bismuth-based layered perovskite Aurivillius phase is such a kind of compounds with formula $(BiFeO_3)_m$-$Bi_4Ti_3O_{12}$, which have been regarded as a promising candidate for RT multiferroics.[8–11] In this structure, the perovskite-type slabs $(Bi_{2+m}Ti_3Fe_mO_{3m+10})^{2-}$ are sandwiched with fluorite-type layers $(Bi_2O_2)^{2+}$ along c axis in a half unit cell. The magnetic transition temperatures of these oxides were reported to be far below RT, i.e., $Bi_5FeTi_3O_{15}$ (80 K), $Bi_6Fe_2Ti_3O_{18}$ (160 K), and $Bi_7Fe_3Ti_3O_{18}$ (190 K).[8] Then substitution with magnetic ions for Fe or raising the number of magnetic layers were employed to enhance the magnetic properties.[12–24] For instance, four-layered $Bi_5FeTi_3O_{15}$ (BFTO) showed good ferroelectricity and a high ferroelectric Curie temperature of 1023 K accompanied by a space group transition from $A2_1am$ to $I4/mmm$.[6] As was reported, substitution with Co for half content of Fe in BFTO can dramatically enhance the magnetic transition temperature far above RT ($\sim$ 618 K), realizing the coexistence of FE and FM at RT.[12,13] And the Co-substituted BFTO showed strong magnetoelectric and magnetodielectric effects.[14] Similarly, obvious ferromagnetism can also be achieved in five-layered $Bi_6FeCoTi_3O_{18}$[15] and $Bi_6Fe_{1-x}Ni_xTi_3O_{18}$;[18] six-layered $Bi_7Fe_{1.5}Co_{1.5}Ti_3O_{21}$[19] and $Bi_7Fe_{3-x}Ni_xTi_3O_{21}$;[23] and seven-layered $Bi_9Fe_{4.7}Me_{0.3}Ti_3O_{27}$ (Me = Ni and Co).[22] These results confirmed that Ni substitution can not only induce ferromagnetism but significantly decrease the leakage current. Moreover, it is worth noting that the content of doped magnetic ions has a great influence on the ferroelectric and magnetic properties. Although the magnetic and dielectric properties of four-layered $Bi_4NdTi_3FeO_{15}$ were investigated,[25,26] their leaky ferroelectric hysteresis loops exhibited poor ferroelectric property. There is still a lack of detailed research on Ni-doped BFTO, such as ferroelectric and magnetic transitions.

In this paper, we prepared $Bi_5Fe_{1-x}Ni_xTi_3O_{15}$ (BFNT-x, $x = 0$, 0.1, 0.2, 0.3, 0.4, 0.5) ceramics by a sol-gel auto-combustion method, and their microstructures, ferroelectric, dielectric, and magnetic properties were investigated in detail. As observed, the Ni content has a major influence on the microstructures and properties of BFTO, and their corresponding mechanisms were discussed. The work may be beneficial to

†Corresponding author. E-mail: hsun@yzu.edu.cn

our designing and exploring single-phase Aurivillius multiferroics.

2. Experimental details

$Bi_5Fe_{1-x}Ni_xTi_3O_{15}$ (BFNT-x, $x = 0$, 0.1, 0.2, 0.3, 0.4, 0.5) ceramics were synthesized by the sol-gel auto-combustion method.[27,28] A detailed process is described as follows. Stoichiometric amounts of $Bi(NO_3)_3{\cdot}5H_2O$ (5 wt% excess) and $Fe(NO_3)_3{\cdot}9H_2O$ were dissolved in 4 M nitric acid solution, and citric acid $C_6H_8O_7{\cdot}H_2O$ was added. Dripping aqueous ammonia (28% mass fraction) into the above solution to adjust pH value to 6–7. Here the molar ratio of metal ions to citric acid was 1:1. The solution was transferred to an oil bath with stirring at 80 °C to obtain dried xerogel. After that, the xerogel was burned at 400 °C for 4 h, followed by ground and pre-sintered at 750 °C for 6 h. The obtained powders were ground again, subsequently pressed into pellets, whose diameter and thickness were 10 mm and 1 mm, respectively. Finally, the pellets were calcined at 900 °C for 4 h in air.

The microstructures of all the samples were analyzed by x-ray diffractometer (XRD, XRD-7000, SHK, Japan), scanning electron microscope (SEM, TESCAN VEGA3, Czech), and Raman scattering spectra (Renishaw, USA). The valence states of ions were investigated by an x-ray photoelectron spectroscopy (XPS, ESCALAB 250Xi, Thermo Fisher Scientific, USA). The magnetic properties were measured by a vibrating sample magnetometer (VSM, EV7, ADE, USA). To test the electrical properties, the calcined pellets were polished to a thickness of about 0.2 mm, and Ag electrodes were deposited on both sides. The ferroelectric properties of the samples were characterized by using a Precision LC ferroelectric analyzer (Radiant Technology product, USA). The dielectric constant and loss tangent dependent on temperature were measured with a broadband dielectric spectrometer (Novocontrol Technologies, Germany). The thermo-magneto-gravimetry (TMG) measurements were performed using thermo-gravimetric analysis (TGA, Q5000IR, USA) technique to measure the samples' weight dependent on temperatures in an applied magnetic field. The measurements were carried out in nitrogen atmosphere with a 0.02 T magnetic field. The ferroelectric transitions were studied by the differential scanning calorimetry (DSC, STA 449 F3 Jupiter, Netzsch, Germany) in the process of a heating and cooling.

3. Results and discussion

Figure 1(a) shows the XRD patterns of the BFNT-x ceramic samples. All the diffraction peaks of all samples can be detected according to the standard PDF file of $Bi_5Fe_1Ti_3O_{15}$ (JCPDS No. 38-1257, space group $A2_1am$). All BFNT-x samples have a four-layered perovskite structure without other identifiable impurity phases,[12–14] which suggests that Ni successfully entered into B-site to replace Fe. To confirm this, the $Bi_5Fe_{0.8}Ni_{0.2}Ti_3O_{15}$ was refined using Topas based on the orthorhombic space group $A2_1am$, as exhibited in Fig. 1(b), and good agreement between the experimental and calculated pattern is obtained with $R_{wp} = 8.11\%$ and $R_p = 6.18\%$.

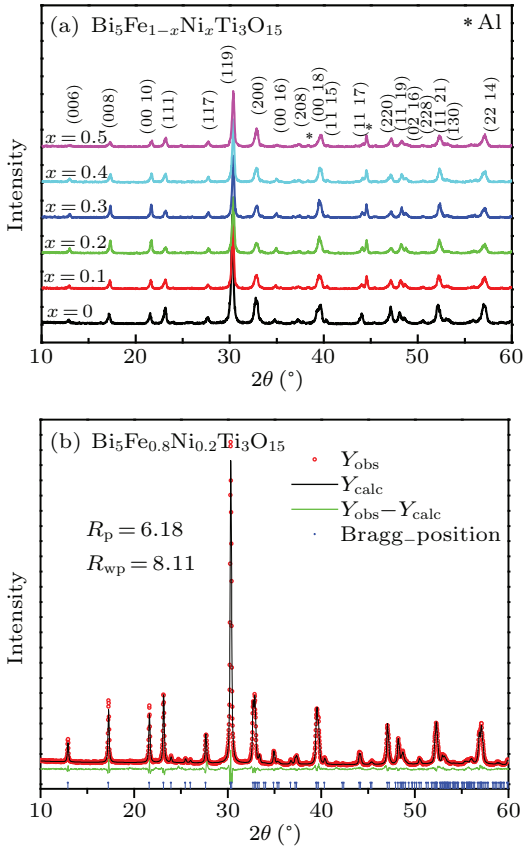

Fig. 1. (a) XRD patterns of $Bi_5Fe_{1-x}Ni_xTi_3O_{15}$ ($x = 0$–0.5) ceramics, and (b) XRD pattern of $Bi_5Fe_{0.8}Ni_{0.2}Ti_3O_{15}$. Circles represent the experimental data, and the calculated data are the continuous line overlapping them. The middle curve indicates the difference between the experimental and calculated data. The lowest vertical bars show the expected reflection.

Raman scattering in the frequency range of 50–1000 cm^{-1} was employed to explore the influences of Ni substitution on the BFTO lattice, as presented in Fig. 2. There are two kinds of Raman modes in layered perovskite compounds, i.e., low frequency modes (below 200 cm^{-1}) and high frequency modes (above 200 cm^{-1}).[29–31] The low frequency mode around 121 cm^{-1} is ascribed to the vibration of heavier Bi ions at A-site. The high frequency modes, i.e., 265 cm^{-1}, 565 cm^{-1}, and 860 cm^{-1} could originate from the stretching and bending of the TiO_6 octahedra, which is similar to those in layer-structured oxides.[32–34] The mode located at 535 cm^{-1} may be associated with the $Fe(Ni)O_6$, which coincides with those of the BFTO (541 cm^{-1}) and $Bi_5Fe_{0.5}Co_{0.5}O_{15}$ (BFCT, 536 cm^{-1}).[35] Compared with BFTO and BFCT, the mode at

705 cm^{-1} may be related to the torsional bending and stretching of Fe(Ni)O_6 octahedra, which moves slightly to the lower frequency. This is due to the substitution of heavier Ni for lighter Fe ions, as the frequency of the vibrating mode is proportional to $\sqrt{(k/M)}$. Here k is the force constant and M is the reduced mass. Interestingly, the other two modes located at 330 cm^{-1} and 828 cm^{-1} may be relevant to the ferroelectric phase and magnetic phase, respectively, because both of them become broaden and disappear with the increasing temperature.[35] All the modes except the one at 705 cm^{-1} do not shift, confirming Ni successful substitution for Fe.

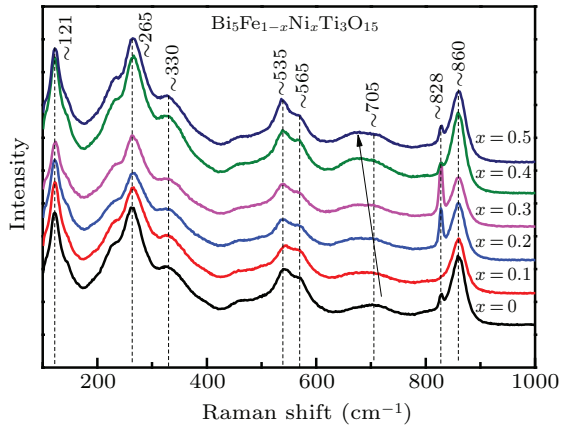

Fig. 2. Raman scattering spectra of BFNT-x ceramics.

Figure 3 displays the surface SEM images of BFCT-x samples. All samples are homogeneous, dense, and randomly oriented, implying good crystallinity. Meanwhile, all the samples have flaky grains with obvious anisotropy. This is the typical characteristics of layered perovskite Aurivillius oxides due to its preferential growth in *ab* plane.[27,28] With the increase of Ni content x, the grain size firstly increases and then decrease, revealing that Ni doping has an effect on the grain growth.

To gain the electronic structure information of elements in the samples, x-ray photoelectron spectroscopy (XPS) of BFNT with $x = 0$, 0.1, 0.3, and 0.5 was carried out, as shown in Fig. 4. According to the report,[36] the Fe $2p_{3/2}$ peaks located at 709.3 eV and 710.7 eV are ascribed to Fe^{2+} and Fe^{3+} ions, respectively. The experimental Fe $2p_{3/2}$ peaks shown in Fig. 4(a) are located at 710.5–910.6 eV, which means there are both Fe^{3+} and Fe^{2+} ions in the samples. Using the Lorentzian–Gaussian fitting and calculating, the atomic ratio of elements can be determined quantitatively by the ratio of area below the corresponding peak. The calculated ratio of Fe^{3+} to Fe^{2+} is listed in Table 1. It can be seen that a small amount of Ni doping ($x < 0.1$) can inhibit the valence variation of Fe ions. As for the spectra of the Ni $2p_{3/2}$ in BFNT-0.3 and BFNT-0.5 (exhibited in Fig. 4(b)), the peaks at 855.1 eV are close to the binding energy of Ni $2p_{3/2}$ in Ni_2O_3, illustrating that the Ni ions are in the ionic state of +3.[37] Normally, the oxygen vacancies may be accompanied with the valence change of cations and affect the electrical and magnetic properties.[38] Therefore, the O 1s core-level spectra were analyzed and presented in Fig. 4(c). The deconvoluted peaks located at 529.7 eV and 531.7 eV are assigned to the lattice oxygen (denoted with $O_{[1]}$) and oxygen vacancies (denoted with $O_{[2]}$),[39,40] respectively. Here the peaks marked with $O_{[3]}$ are attributed to the absorbed oxygen species. The relative amount of oxygen vacancies can be qualitatively ascertained by $I_{O[2]}/I_{O[1]}$, as shown in Table 1. It is concluded that Ni substitution can largely improve the stability of oxygen ions and reduce the oxygen vacancy concentration.

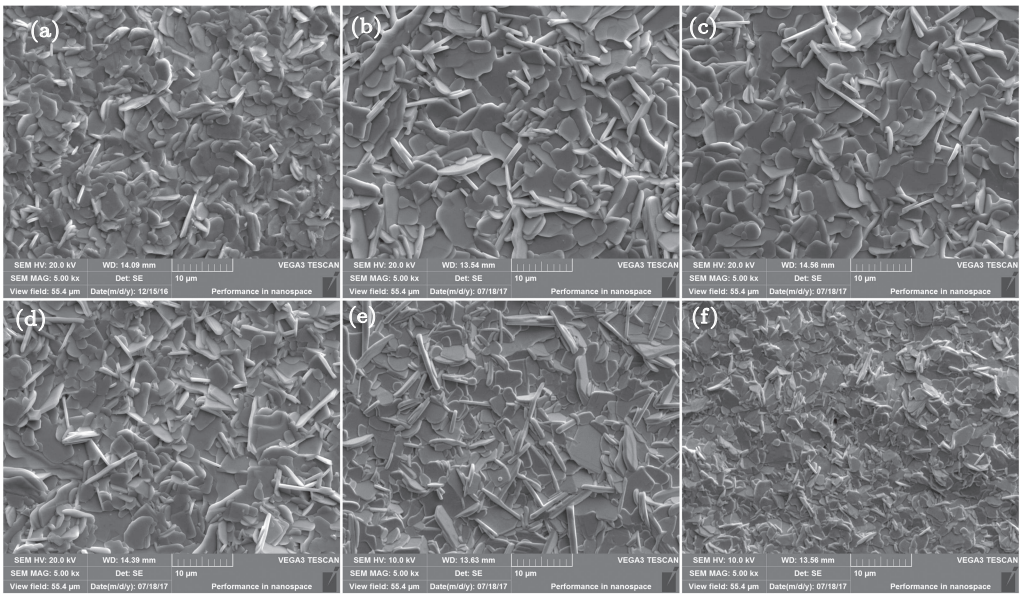

Fig. 3. Surface SEM images of BFNT-x samples for (a) $x = 0$, (b) $x = 0.1$, (c) $x = 0.2$, (d) $x = 0.3$, (e) $x = 0.4$, and (f) $x = 0.5$.

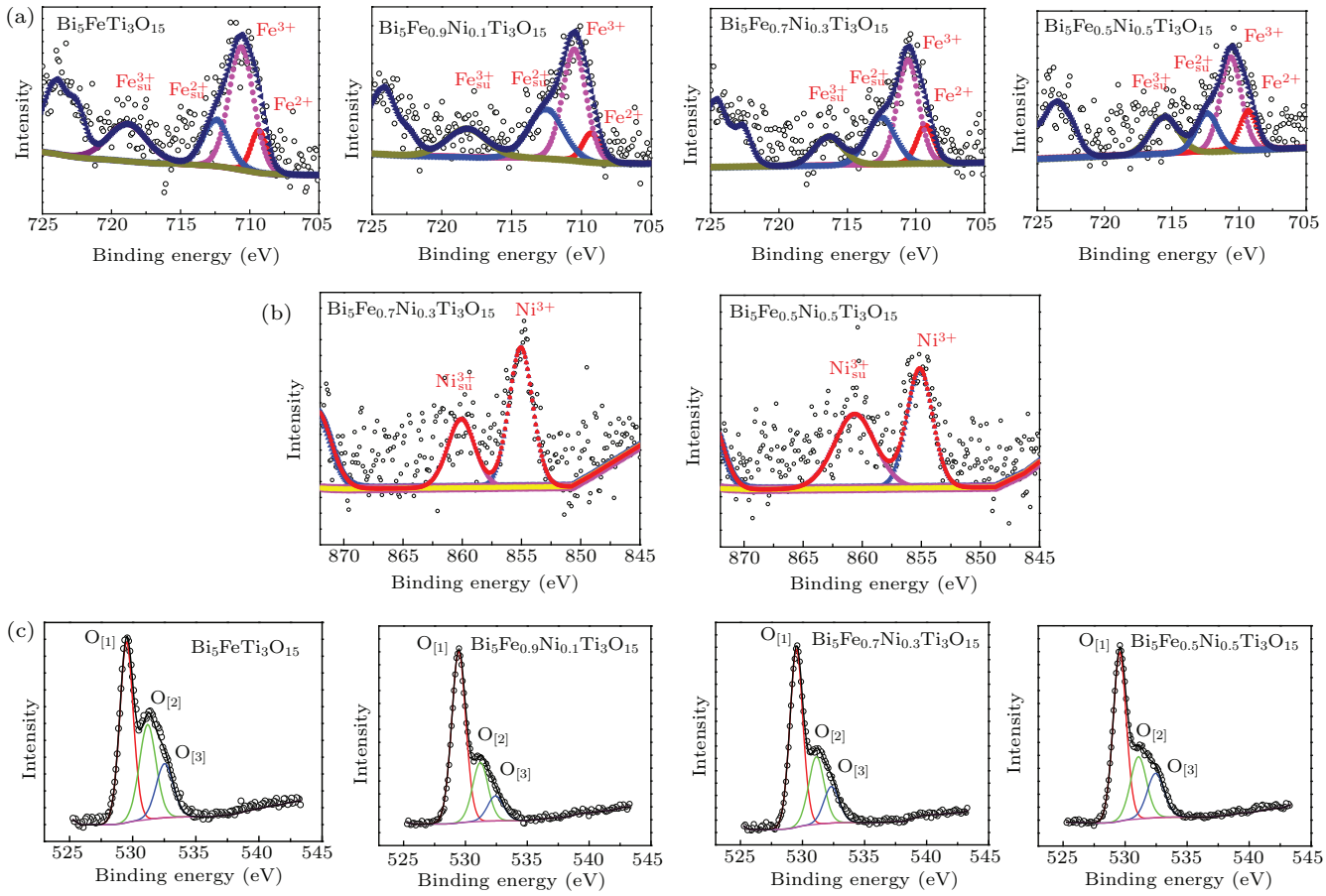

Fig. 4. 4 High resolution XPS spectra and fitted curve of (a) Fe 2p, (b) Ni 2p, and (c) O 1s of BFNT-x.

Table 1. The calculated atomic ratios of Fe^{2+}/Fe^{3+} and $I_{O[2]}/I_{O[1]}$ dependent on Ni content.

x	0	0.1	0.3	0.5
Fe^{2+}/Fe^{3+}	0.22	0.19	0.3	0.36
$I_{O[2]}/I_{O[1]}$	0.6	0.46	0.46	0.45

Figure 5(a) exhibits the magnetic hysteresis M–H curves of all samples measured at RT, and their enlarged view of central parts are shown in the inset. For $x = 0$, 0.4, and 0.5 samples, the linear M–H plots imply the feature of antiferromagnetism (AFM) or para-magnetism (PM). The other M–H plots exhibit typical hysteresis, which clearly indicate the presence of FM moment. However, the magnetization is not saturated even under the higher magnetic field ~ 1 T, revealing that there also exist AFM interactions in these samples. Figure 5(b) summarizes the dependence of remnant magnetization ($2M_r$) and saturated magnetization (M_s) on Ni content. With the increase of Ni content, both of them firstly increase ($x \leq 0.2$) and then decrease with further more Ni content. The changing trend of the magnetism with increasing Ni content is consistent with that of $Bi_7Fe_{3-x}Ni_xTi_3O_{21}$ ceramics.[23] When $x = 0.2$, $2M_r$ and M_s reach the maximum of 0.24 emu/g and 0.68 emu/g, respectively. In this kind of oxides, the magnetism may be mainly affected by the following factors. Firstly, the Fe (Ni)–O_6 octahedral tilting and distorted crystal structure would bring about canted spin structure. And spin canting of AFM coupling of Fe–O and Ni–O sublattices based on Dzyaloshinsky–Moriya (DM) interactions leads to the present weak ferromagnetism.[15,16,18–24] Secondly, there exist oxygen vacancies in the samples confirmed in XPS results. The magnetic ions are apt to integrate with oxygen vacancies to form the bound magnetic polarons (BMPs), and the interactions between BMPs are ferromagnetic.[41] As discussed above, the oxygen vacancy concentration was depressed by Ni doping, which would decrease this kind of ferromagnetic interactions. Both the aspects above result in the variation of the magnetic properties dependent on Ni content.

To clarify the magnetic interactions in BFNT, the dependence of the sample's weight under a magnetic field on temperature was investigated. Figure 6 gives thermo-magneto-gravimetry (TMG) and the corresponding differential thermo-magneto-gravimetry (DTMG) curves of BFNT-x samples with $x = 0.1$, 0.2, and 0.3. Each sample has only one peak, which corresponds to the FM-to-PM phase transition. This means that there does not exist other magnetic impurity phase, demonstrating that the room-temperature weak FM comes from single-phase BFNT. The peaks of BFNT-0.1, BFNT-0.2, and BFNT-0.3 at approximately 824 K, 796.3 K, and 774 K, respectively, are far above RT, leading to the occurrence of weak ferromagnetism at RT. The magnetic transition tempera-

ture decreases as the Ni content increases. Generally, the two main factors affecting magnetic transition temperature include lattice distortion and magnetic interaction. Less Ni substitution ($x \leq 0.1$) can dramatically enhance the magnetic transition temperature from 80 K to 824 K and realize the weak ferromagnetism at RT. More Ni content ($x > 0.1$) decreases the magnetic transition temperature, which may be ascribed to the decreased order of the B-site ions and the relative stability of the magnetic structure.[42] As for the lattice distortion, it is affected by the changes of the bond angle and length between coupling magnetic ions, which is also related to the transition temperature from FE to paraelectric phase transition.[14] As reported, the higher ferroelectric transition temperature means the larger structural distortion. Therefore, we will discuss the temperature dependence of the dielectric properties and DSC curves of all samples below.

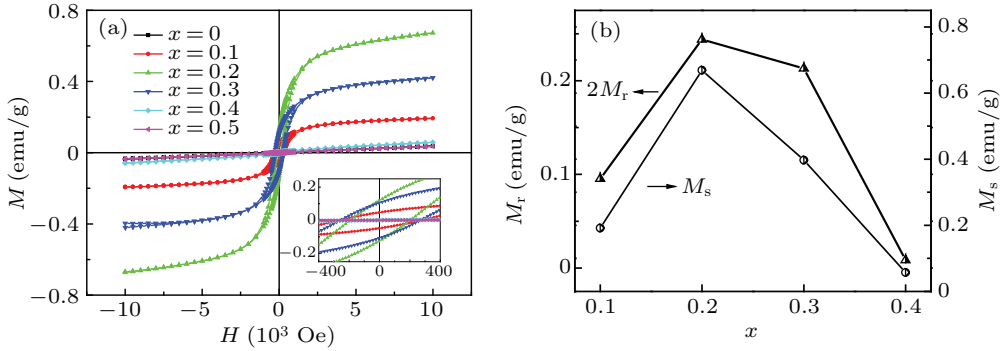

Fig. 5. (a) Magnetic hysteresis M–H curves measured at RT of SBNT-x samples. (b) The variation of $2M_r$ and M_s with Ni doping content.

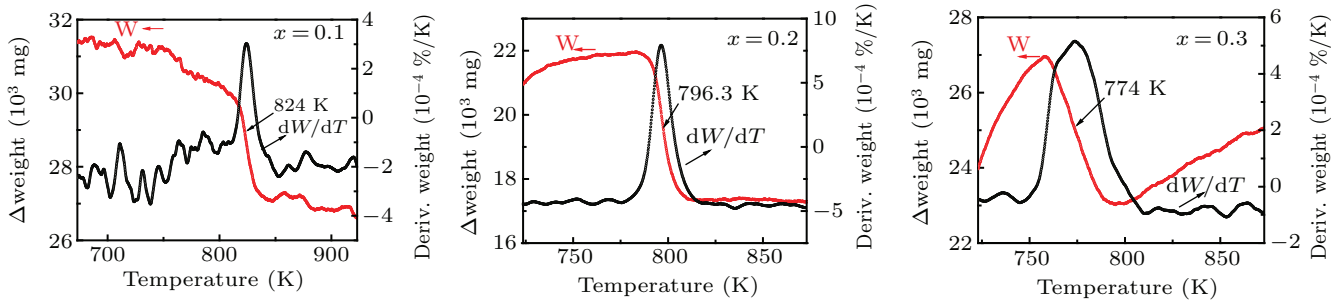

Fig. 6. Weight loss under a magnetic field and DTMG curves of BFNT samples with $x = 0.1$, 0.2, and 0.3.

Figure 7 shows the temperature dependence of dielectric constant ε and loss tan δ of all BFNT samples from 370 K to 1080 K at different frequencies. All the samples exhibit a similar behavior, and a set of anomalies are observed around 600 K and marked with rectangle. The set of dielectric peak locations of dielectric constant and loss shift toward higher temperature with the increase of frequency, exhibiting a typical thermal-activated relaxation behavior. Whereas, it is difficult to determine the dielectric peak position due to the wide dielectric loss peak. In order to understand the mechanism of this abnormal dielectric behavior, the temperature dependent imaginary part M'' of dielectric modulus for BFNT was studied, depicted in Fig. S1. According to the point defect relaxation theory, the activation energy E_a of relaxation units can be calculated by the Arrhenius law $f_r = f_\infty \exp(E_a/k_B T)$, where f_r and f_∞ are the relaxation frequencies of characteristic peak and at infinite temperature, respectively. T is the temperature of the M''-peak, and k_B is the Boltzmann constant. As displayed in Fig. S2, the activation energies E_a are evaluated to be 0.85 eV, 0.56 eV, 0.57 eV, 0.56 eV, 0.60 eV, and 0.55 eV for the BFNT samples with $x = 0$, 0.1, 0.2, 0.3, 0.4, and 0.5, respectively. These values are close to the migration energy of oxygen vacancies (0.5–1.1 eV),[43,44] indicating that these dielectric anomalies around 600 K are associated with the hopping process of oxygen vacancies. Unfortunately, the FE Curie temperature is not found in the dielectric spectra dependent on temperature from 370 K to 1080 K due to the limit of the dielectric spectrometer. Then DSC traces of all BFNT samples will be studied as follows.

Figure 8 shows the DSC curves of all BFNT samples. There are two sets of endothermic peaks on heating and two sets of exothermic peaks on cooling for each sample, indicating reversibility of transitions. Both the sets of peaks exhibit thermal hysteresis. For the BFTO sample, the low-temperature endothermic peak located at 1030 K with its corresponding exothermic peak at 1020 K is in a good agreement with the ferroelectric transition accompanied with structural transition from orthorhombic to tetragonal phase.[45] The other high-temperature endothermic peak at 1126 K with its corresponding exothermic peak at 1083 K originates from the lattice expansion of the tetragonal phase. We summarize the temper-

ature of all endothermic and exothermic peaks in Table 2, and define the transition temperature as the average value of the temperature of endothermic and corresponding exothermic peaks. From Table 2, it can be seen that the ferroelectric transition temperature decreases with the increasing Ni content, implying lessen structural distortion.

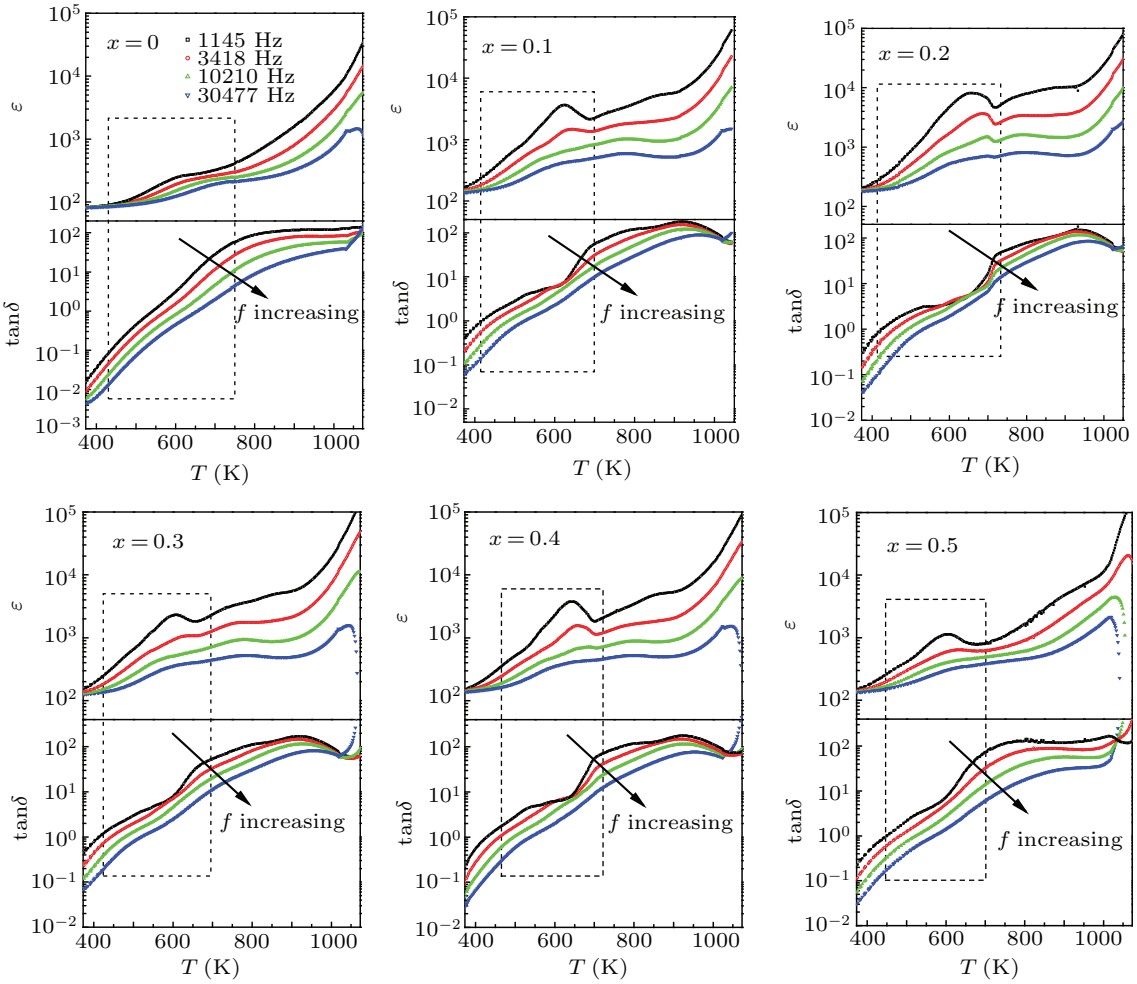

Fig. 7. The temperature dependence of dielectric constant ε and loss tan δ of all BFNT samples ranging from 370 K to 1050 K at different frequencies.

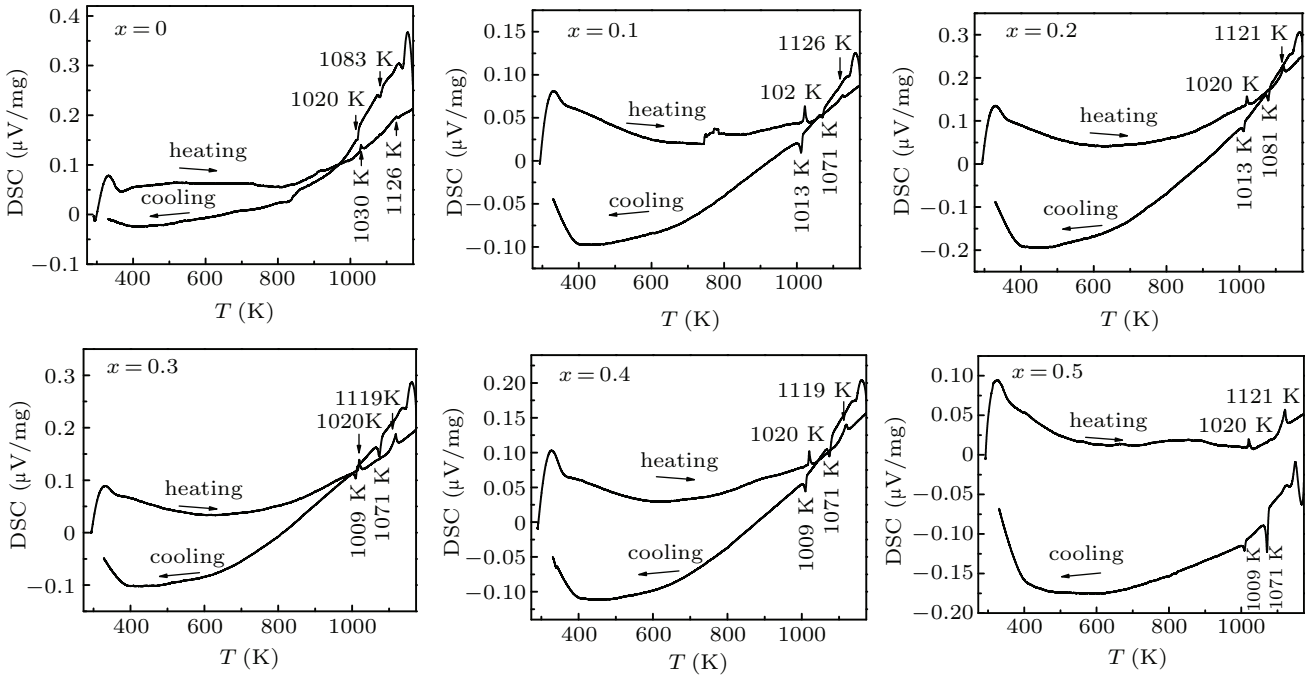

Fig. 8. DSC curves of all BFNT samples.

Table 2. The detected transition temperature of all BFNT samples.

x	$T_{heating}$ (K)	$T_{cooling}$ (K)	T_1 (K)	$T_{heating}$ (K)	$T_{cooling}$ (K)	T_2 (K)
0	1030	1020	1025	1126	1083	1104.5
0.1	1022	1013	1017.5	1126	1071	1098.5
0.2	1020	1013	1016.5	1121	1081	1101
0.3	1020	1009	1014.5	1119	1075	1097
0.4	1020	1009	1014.5	1119	1075	1097
0.5	1020	1009	1014.5	1121	1071	1096

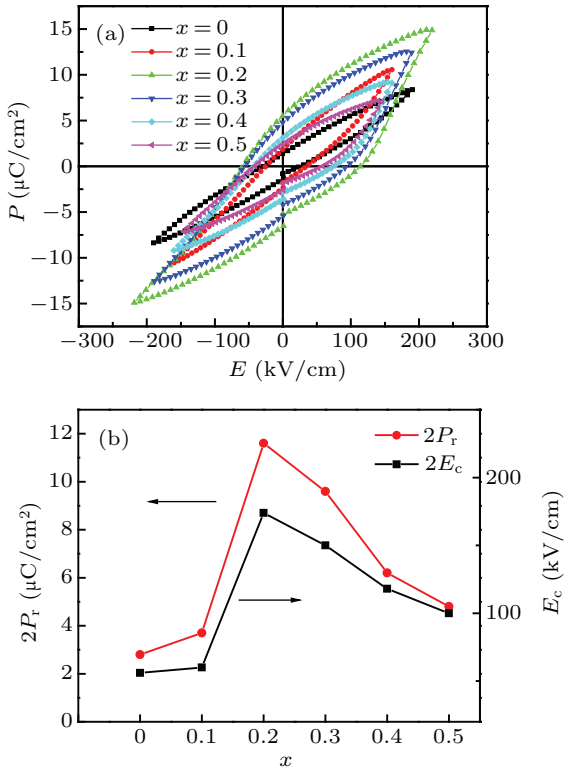

Fig. 9. (a) Polarization versus electric field (P–E) hysteresis loops of BFNT. (b) The variation of remnant polarization ($2P_r$) and coercive field (E_c) dependent on Ni content.

Finally, the ferroelectric hysteresis loops of all samples were measured at RT, as illustrated in Fig. 9. For the BFTO, its loop shows round and leaky. After Ni substitution, the ferroelectric remnant polarization as well as the breakdown electric field enhance largely. The values of remnant polarization ($2P_r$) and coercive field (E_c) firstly increase and then decrease with the increase of Ni content. When $x = 0.2$, the $2P_r$ reaches the largest value about 11.6 μC/cm^2, and the breakdown field also achieves the maximum of 220 kV/cm. As is well known, the ferroelectric property may be related to the following factors: (1) Structural distortion.[46,47] The substitution of Fe by larger radius ions, i.e., Co and Ni, can reduce the displacement of the B-site ions, decreasing the structural distortion. The decreased structural distortion leads to the reduced FE Curie temperature, which is confirmed in Fig. 8. The decrease structural distortion will reduce the larger remnant polarization. (2) Oxygen vacancy.[48] It was reported that oxygen vacancies usually aggregate at the ferroelectric domain walls and pin the domain switching, resulting in deterioration of the remnant polarization. Ni substitution decreases oxygen vacancy concentration discussed above and increases the polarization. (3) Grain size.[49] Larger grain can weaken the aggregation of the defects at the domain walls, lessening the pining of the domain walls and enhancing the remnant polarization. As shown in Fig. 2, less Ni substitution increases grain size, which can enhance the remnant polarization. The above three factors bring about the variation of ferroelectricity dependent on Ni content.

4. Conclusions

The microstructures, ferroelectric, magnetic, and dielectric properties of BFNT-x ceramics were investigated systematically. XRD and Raman spectra confirmed that Ni substitution does not change the four-layered perovskite structure. Ni substitution can improve ferroelectricity as well as magnetic properties. The largest remnant polarization ($2P_r \sim$ 11.6 μC/cm^2) and the highest remnant magnetization ($2M_r \sim$ 0.244 emu/g) were found in the BFNT-0.2 sample. The weak FM of the doped samples may mainly originate from the spin canting of Fe/Ni-based sublattices via the antisymmetric DM interaction. The enhancement of FE and magnetic properties is related to the structural distortion. Therefore, DSC tests were performed, detecting FE transition and lattice expansion of the tetragonal phase. The dielectric relaxation behaviors were observed in all samples, which may be caused by the migration of oxygen vacancies due to thermal activation. The present work is helpful for design of room-temperature multiferroics based on Aurivillius phase.

References

[1] Schmid H 1994 *Ferroelectrics* **162** 317
[2] Eerenstein W, Mathur N and Scott J 2006 *Nature* **442** 759
[3] Ramesh R and Spaldin N 2007 *Nat. Mater.* **6** 21
[4] Qin M H, Lin L, Li L, Jia X T and Liu J M 2015 *Chin. Phys. B* **24** 037509
[5] Zhou L, Wang X, Zhang H M, Shen X D, Dong S and Long Y W 2018 *Acta Phys. Sin.* **67** 157505 (in Chinese)
[6] Snedden A, Hervoches C and Lightfoot P 2003 *Phys. Rev. B* **67** 092192
[7] Pan Q and Chu B J 2020 *Chin. Phys. B* **29** 087501
[8] Li J, Huang Y, Jin H, Rao G and Liang J 2013 *J. Am. Ceram. Soc.* **96** 3920
[9] Zhao H Y, Kimura H, Cheng Z X, Osada M, Wang J L, Wang X L, Dou S X, Liu Y, Yu J D, Matsumoto T, Tohei T, Shibata N and Ikuhara Y 2014 *Sci. Rep.* **4** 5255
[10] Birebaum A Y and Ederer C 2014 *Phys. Rev. B* **90** 214109
[11] Zhai X F, Yun Y, Meng D C, Cui Z Z, Huang H L, Wang J L and Lu Y L 2018 *Acta Phys. Sin.* **15** 157702 (in Chinese)

[12] Sun H, Lu X M, Xu T T, Su J, Jin Y M, Ju C C, Huang F Z and Zhu J S 2012 *J. Appl. Phys.* **111** 124116

[13] Mao X Y, Wang W, Chen X B and Lu Y L 2009 *Appl. Phys. Lett.* **95** 082901

[14] Mao X Y, Sun H, Wang W, Chen X B and Lu Y L 2013 *Appl. Phys. Lett.* **102** 072904

[15] Liu Z, Yang J, Tang X W, Yin L H, Zhu X B, Dai J M and Sun Y P 2012 *Appl. Phys. Lett.* **101** 122402

[16] Yang J, Yin L, Liu Z, Zhu X, Song W, Dai J, Yang Z and Sun Y 2012 *Appl. Phys. Lett.* **101** 012402

[17] Srinivas A, Suryanarayana S, Kumar G and Mahesh K 1999 *J. Phys. Condens. Matter* **11** 3335

[18] Xiong P, Yang J, Qin Y, Huang W, Tang X, Yin L, Song W, Dai J, Zhu X and Sun Y 2017 *Ceram. Int.* **43** 4405

[19] Wang J, Li L, Peng R, Fu Z, Liu M and Lu Y 2015 *J. Am. Ceram. Soc.* **98** 1528

[20] Wang J, Fu Z, Peng R, Liu M, Sun S, Huang H, Li L, Knize R and Lu Y 2015 *Mater. Horiz.* **2** 232

[21] Lei Z, Liu M, Ge W, Li Z, Knize R and Lu Y 2015 *Mater. Lett.* **139** 348

[22] Wang G P, Sun S J, Huang Y, Wang J L, Peng R R, Fu Z P and Lu Y L 2014 *Chin. Sci. Bull.* **59** 5199

[23] Sun S J, Ling Y H, Peng R R, Liu M, Mao X Y, Chen X B, Knize R J and Lu Y L 2013 *RSC Adv.* **3** 18567

[24] Sun S J, Huang Y, Wang G P, Wang J L, Fu Z P, Peng R R, Knize R J and Lu Y L 2014 *Nanoscale* **6** 13494

[25] Chen X, Xiao J, Yao J, Kang Z, Yang F and Zeng X 2014 *Ceram. Inter.* **40** 6815

[26] Chen X, Xiao J, Xue Y, Zeng X, Yang F and Su P 2014 *Ceram. Inter.* **40** 2635

[27] Sun H, Lu Y X, Xie X, Yao T S, Xu Z R, Wang Y and Chen X B 2019 *J. Eur. Ceram. Soc.* **39** 2103

[28] Lu Y X, Sun H, Wang Z F, Xie X, Yao T S, Wang J L, Qi Y J, Chen X B and Lu Y L 2020 *J. Mater. Sci.: Mater. Electron.* **31** 1034

[29] Shao C, Lu Y, Wang D and Li Y 2012 *J. Eur. Ceram. Soc.* **32** 3781

[30] Kojima S, Imaizumi R, Hamazaki S and Takashige M 1994 *Jpn. J. Appl. Phys.* **33** 5559

[31] Graves P, Hua G, Myhra S and Thompson J 1995 *J. Solid State Chem.* **114** 112

[32] Kojima S, Imaizumi R, Hamazaki S and Takashige M 1994 *Jpn. J. Appl. Phys.* **33** 5559

[33] Graves P R, Hua G, Myhra S and Thompson J G 1995 *J. Solid State Chem.* **114** 112

[34] Wang J, Cheng G, Zhang S, Cheng H and Chen Y 2004 *Phys. B* **344** 368

[35] Mao X, Wang W, Sun H. Lu Y L and Chen X B 2012 *Integrated Ferroelectrics* **132** 16

[36] Huang F, Lu X, Wang Z, Lin W, Kan Y, Bo F, Cai W and Zhu J 2009 *Appl. Phys. A* **97** 699

[37] Mansour A N 1994 *Surf. Sci. Spectra* **3** 231

[38] Yang R X, Lu Y M, Zeng L Z, Zhang L J and Li G N 2020 *Acta Phys. Sin.* **69** 107701 (in Chinese)

[39] Kashinath A, Mukesh N, Meenal S, Nagarajan V and Satishchandra B 2009 *Appl. Phys. Lett.* **95** 203502

[40] Lin Y, Yang Y, Zhuang B, Huang S, Wu L, Huang Z, Zhang F and Du Y 2008 *J. Phys. D Appl. Phys.* **41** 195007

[41] Ti R, Lu X, He J, Huang F, Wu H, Mei F, Zhou M, Li Y, Xu T and Zhu J 2015 *J. Mater. Chem. C* **3** 11868

[42] Lei Z, Chen T, Li W, Liu M, Ge W and Lu Y 2017 *Crystals* **7** 76

[43] Scott J and Dawber M 2000 *Appl. Phys. Lett.* **76** 3801

[44] Yao Y, Song C, Bao P, Su D, Lu X M, Zhu J S and Wang Y N 2004 *J. Appl. Phys.* **95** 3126

[45] Li J, Huang Y P, Rao G H, Liu G Y, Luo J, Chen J R and Liang J K 2010 *Appl. Phys. Lett.* **96** 222903

[46] Liu J, Bai W, Yang J, Xu W, Zhang Y, Lin T, Meng X, Duan C, Tang X and Chu J 2013 *J. Appl. Phys.* **114** 112903

[47] Ahn S, Noguchi Y, Miyayama M and Kudo T 2000 *Mater. Res. Bull.* **35** 825

[48] Kim J, Raghavan C and Kim S 2015 *Ceram. Int.* **41** 1567

[49] Jiang Q Y, Subbarao E C and Cross L E 1994 *J. Appl. Phys.* **75** 7433